Revista Brasileira de Aplicações de Vácuo, v. 25, n. 1, 24-30, 2006.

TiO_2 FILMS PRODUCED BY ELECTRON BEAM VACUUM DEPOSITION FROM NANOMETRIC POWDER OBTAINED BY PECHINI'S METHOD

F.S. De Vicente[1*]; M.I.B. Bernardi[1]; F.L. Leite[1,2]; P.S.P. Herrmann[2]; A.C. Hernandes[1]
[1]Instituto de Física de São Carlos, USP, CP 369, São Carlos, SP, 13560-970, Brasil
[2]Embrapa Instrumentação Agropecuária, CP 741, São Carlos, SP, 13560-970, Brasil

Received: July 27, 2005; Revised: March 31, 2006

Keywords: nanometric powder, TiO_2 films, electron beam evaporation, vacuum deposition.

ABSTRACT

Nanometric TiO_2 powders were obtained from low temperature calcination of a TiO_2 resin prepared using the Pechini's method. Firing the TiO_2 resin at 500 ^oC/2h a powder with anatase phase was obtained, otherwise firing the TiO_2 resin at 700 ^oC/2h a powder with rutile phase was achieved as measured by X-ray diffraction (XRD). The anatase powder presented average particle size of 60 nm observed by Scanning Electronic Microscopy (SEM-FEG) micrographs and average crystallite size of 13 nm calculated from the XRD, while the rutile powder presented average crystallite size of 34 nm. Nanocrystalline TiO_2 films with good homogeneity and optical quality were obtained with 80 nm and 320 nm in thickness by Electron Beam Physical Vapour Deposition (EB-PVD) in vacuum on amorphous quartz substrates submitted at 350^oC during the evaporation. The 80 nm-thick film presented average particle size of 140 nm and roughness (R_a) of 1.08 nm and the 320 nm-thick film showed average particle size of 350 nm and roughness (R_a) of 2.14 nm measured by Atomic Force Microscopy (AFM). In these conditions of deposition the films presented only anatase phase observed by XRD and MicroRaman spectroscopy.

1. INTRODUCTION

Since the discovery of the photoinduced hidrophilicity of TiO_2 films, this material attracted attention because of its application in antifogging mirror and glasses [1]. Also the TiO_2 posses high photocatalytic activity, excellent chemical and photochemical stability, and superior oxidation capacity favouring its application in photoelectrochemical devices, and nonlinear optical systems [2-5]. Additionally, their outstanding tissue compatibility and hemocompatibility [6,7] ensure a continuous strong interest from the biomedical community. Nanometer-sized TiO_2 has recently gained a considerable amount of attention because of their unique physical and chemical properties and their importance in technological applications including ultraviolet light absorbers, photocatalysts, gas sensors, etc. [8-14]. A significant motivation of current research into nanometer-sized TiO_2 powder and film is the need to develop an understanding of the relationships between their structures and properties associated with nanometer-sized grains. Nanostructured TiO_2 is extensively studied in the field of solar cells. Additionally, for solar cell applications, the anatase structure is preferred over the rutile structure, as anatase exhibits a higher electron mobility, lower dielectric constant, lower density, and lower deposition temperature. In solar cells associated with organic dye molecules the use of nanostructured TiO_2 films overcomes the problem of high resistance, because the increased surface area ensures enough dye absorption to absorb all the light and provides short-range contact between dye and oxide [15].
The powder preparation method used in this work play an important role in the facility of obtaining nanometric powders compared with other methods such as reactive TiOH [16], sol-gel [17], and modified hydrolysis reaction [18]. The obtaining of the TiO_2 phase and particle size desired can be controlled by the temperature and pH of the precursor TiO_2 resin, respectively.
In this article we report the synthesis of nanometric TiO_2 powder using low temperature calcinations of a precursor TiO_2 resin prepared by the Pechini's method. Also the production and characterization of nanocrystalline TiO_2 thin films deposited by electron beam in vacuum is presented. The TiO_2 resin, powders and films obtained were mainly characterized by Differential Thermal Analysis (DTA), Optical Transmittance, MicroRaman Spectroscopy, Scanning Electron Microscopy with Field Emission Gun (SEM-FEG), Atomic Force Microscopy (AFM), and X-ray Diffraction (XRD).

2. EXPERIMENTAL

2.1 Nanometric TiO_2 Powder Preparation

Details of the nanometric TiO_2 powder synthesis used in this study is outlined in the flow chart of Figure 1. The raw materials used for TiO_2 synthesis, were titanium isopropoxide (98.0 % Aldrich), Ethylene glycol (99.9 % Merk), and Citric acid (99.0% Merk). Titanium citrates were formed by dissolution of titanium isopropoxide in a water solution of citric acid (60-70^oC). The molar fraction of titanium isopropoxide added to citric acid is calculated

* vicente@if.sc.usp.br

regarding the final TiO_2 mass desired. After homogenization of the Ti solution, ethylene glycol was added to promote polymerization of the mixture by polyesterification reaction.

The molar ratio among the citric acid/metal ratio was fixed at 6:1 and the citric acid/ethylene glycol ratio was fixed at 60:40 (mass ratio). The resin was heated at 140°C to eliminate excess of water. The heat treatments to obtain the TiO_2 powder were carried out in two stages: initial heating of the resin at 400°C/4h at 10°C/min to pyrolise the organic material, followed by heating at 500°C/2h or 700°C/2h at 10°C/min, to eliminate residual organic material and formation of the desired TiO_2 phase.

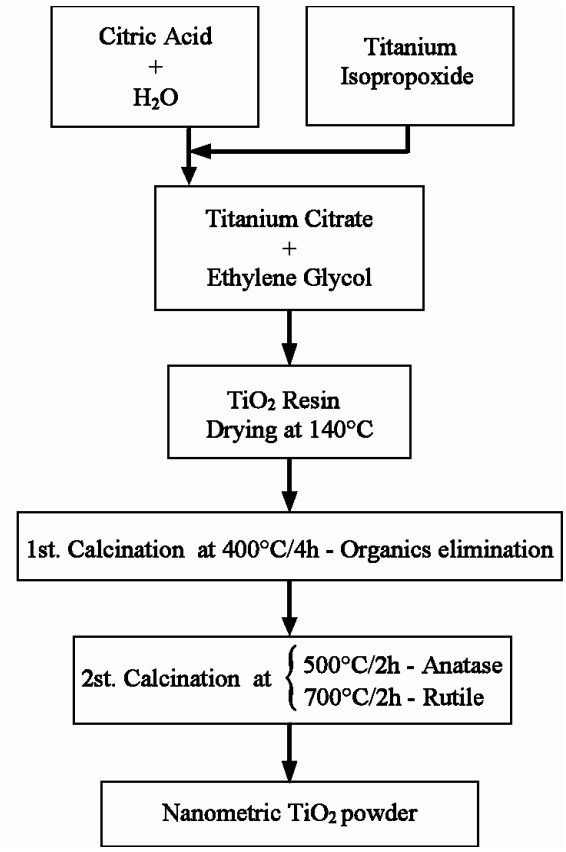

Figure 1 – Preparation route of the TiO_2 resin using the Pechini´s method

2.2 TiO_2 Films Deposition

The TiO_2 films deposition was carried out in an electron beam evaporation system with a pressure of $4x10^{-6}$ Torr [19]. The films were obtained with the electron beam gun (Telemark-231) operating at 7 kV and electron beam with 50 mA. Deposition rates of ~1.0 Å/s were achieved, monitored by a quartz crystal oscillator (Sycon, STM-100). Using this setup we deposited 320 nm-thick and 80 nm-thick films on amorphous quartz substrates submitted at 350°C during the evaporation. The thickness of the films was measured by a Talystep Taylor-Hobson profiler. Tantalum crucibles were used to support the high temperature achieved during the evaporation of the TiO_2 pellet. More details of the EB-PVD system is described elsewhere [20].

2.3 XRD

The crystallinity and phase of the TiO_2 powder and films were investigated by XRD technique using a Rigaku Dmax-2500PC diffractometer operating with Cu K_α radiation. For films was used X-ray grazing angle incidence fixed at 2.0° between the X-ray beam and the film surface, and 2θ detector scanning from 20° to 60°.

2.4 Microscopy Measurements

Scanning electron micrographs (SEM-FEG) were taken by a Zeiss (DSM-940A) scanning electron microscope equipped with field emission gun, allowing 100 KX of magnification. The Atomic Force Microscopy (AFM) images were obtained using a Discoverer TMX 2010 microscope from Topometrix. A pyramidal silicon tip with radius of 25 nm was used in all measurements carried-out in contact mode. The scan area was 5x5 μm consisting of 500 lines which were scanned at a rate of 2 Hz, to measure the topography, grain size and the surface roughness of the TiO_2 films. The image analysis and average roughness (R_a) measurements were calculated using WSxM 4.0 software from Nanotech Electronica S.L. (copyright© November 2003).

2.5 DTA

The resin, after dehydrated, was subjected to thermal analysis using a STA 409 Nestzch Model thermoanalyzer. The sample (50mg) was put into alumina crucibles, using calcined alumina as the reference material. The heating rate was 10^oCmin^{-1} and the thermal analysis was carried out in flowing synthetic air.

2.6 Optical Measurements

The UV-VIS spectra of the TiO_2 films were collected in transmittance mode in a Cary-17 spectrophotometer, in the 250-1500 nm region. Quartz substrates were placed in the reference beam to simultaneously subtract the quartz spectra from the films spectra. The Raman spectra were obtained in a Renishaw MicroRaman Spectrophotometer, coupled to an optical microscope that focuses the incident radiation in ~1.0 μm spot. A He-Ne laser (λ=632.8 nm) was used, with incidence power of 2 mW over the 1000-100 cm^{-1} region.

3. RESULTS AND DISCUSSION

3.1 Nanometric TiO_2 Powder Characterization

As mentioned above in section 2.1, the nanometric TiO_2 powders were prepared following the Pechini's method,

through the reaction of titanium isopropoxide with citric acid and ethylene glycol (Figure 1). After the synthesis and removal of the excess of water, the thermal behavior of the TiO_2 resin was investigated analysed by DTA and the result is shown in Figure 2.

The curve behavior from 25 °C up to 200 °C is due to water loss. The endothermic peak at 256 °C is attributed to loss of water linked to the polymeric chains and the exothermic peak at 336 °C is due to the pyrolise of the polymeric chain structure of citric acid and ethylene glycol.

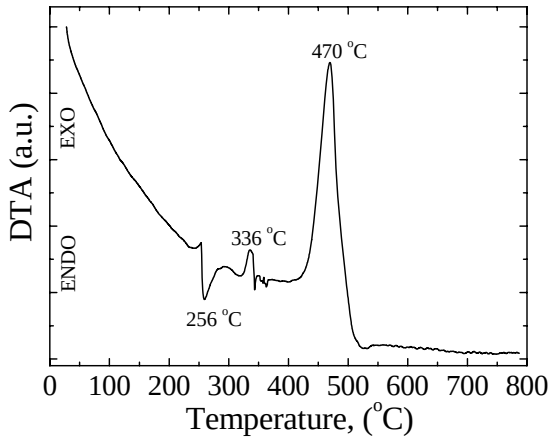

Figure 2 – DTA of the TiO_2 resin.

The strong exothermic peak at 470 °C is attributed to the anatase phase transition in the titanium oxide [21]. The anatase-rutile phase transition peak after 600 °C could not be detectable.

The Figure 3 presents the SEM-FEG micrograph of the anatase TiO_2 powder obtained from the TiO_2 resin calcined at 500°C/2h. The top image corresponds to magnification of 50.000X (200 nm scale) and the bottom image 100.000X magnification, (100 nm scale).It is know that powders with nanometric particles are thermodynamically unstable due to the large surface area. It means that the small dimension particles possess high surface energy, leading the TiO_2 powder agglomerate severely. This behaviour can be visualized in the SEM-FEG micrographs of the anatase TiO_2 powder presented in the Figure 3. Through software analysis of the micrographs the average dimension of these particles was found to be 60 nm. Also, sintering onset can be observed in Figure 3, due to some neck formation between particles.

According with Grosa *et. al*. [22], kinetically sintering and/or coarsening of nanopowders are significantly enhanced. Nanoparticles can adopt different surface energies, for instance, by a different local atomic arrangement at the surface. Therefore, sintering of numerous real nanoparticles indicated depressed sintering onset temperatures (0.2-0.3 T_m) as compared to conventional powders (0.5-0.8 T_m). Consequently, some other sintering mechanisms related to nanopowders have been suggested: dislocation motion, particle rotation, viscous flow, and particle boundary slip.

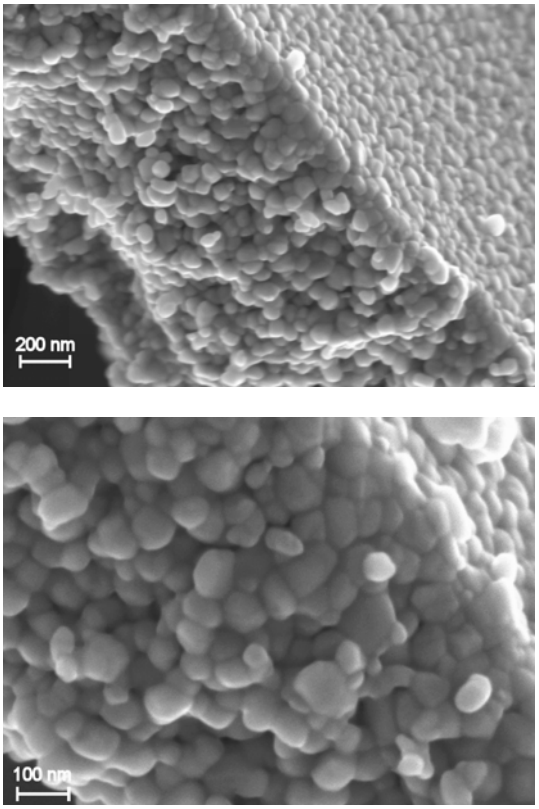

Figure 3 – SEM-FEG micrograph of the anatase TiO_2 powder obtained from the TiO_2 resin calcined at 500°C/2h. Top image: 200 nm scale, 50.000X magnification; Bottom image: 100 nm scale, 100.000X mag.

The Figure 4 shows the XRD pattern of the anatase and rutile TiO_2 powders obtained from the calcination of the TiO_2 resin at 500 °C/2h and 700°C/2h, respectively. The broad peaks observed in the anatase XRD pattern (fig. 4-a) indicates small average crystallite diameter, which was estimated by the Scherrer's equation as ~13 nm. On the other side, the rutile XRD pattern (fig. 4-b) presents sharp peaks (estimated average crystallite diameter ~ 34 nm), compared with the anatase XDR pattern. This is attributed to the higher calcination temperature of the TiO_2 resin to obtain rutile phase (700°C/2h), leading to the growth of the crystallites. It is important to note that the temperature range used in this work (500°C-700°C) to obtain the TiO_2 phase is low compared with conventional TiO_2 powders, where rutile phase formation and sintering of the particles occurs above 1000°C. Concerning the anatase and rutile phase formation at low temperatures (500°C-700°C) using the Pechini's method, we can also consider the high energy releasing in the pyrolise reaction of the organics during the firing of the TiO_2 resin.

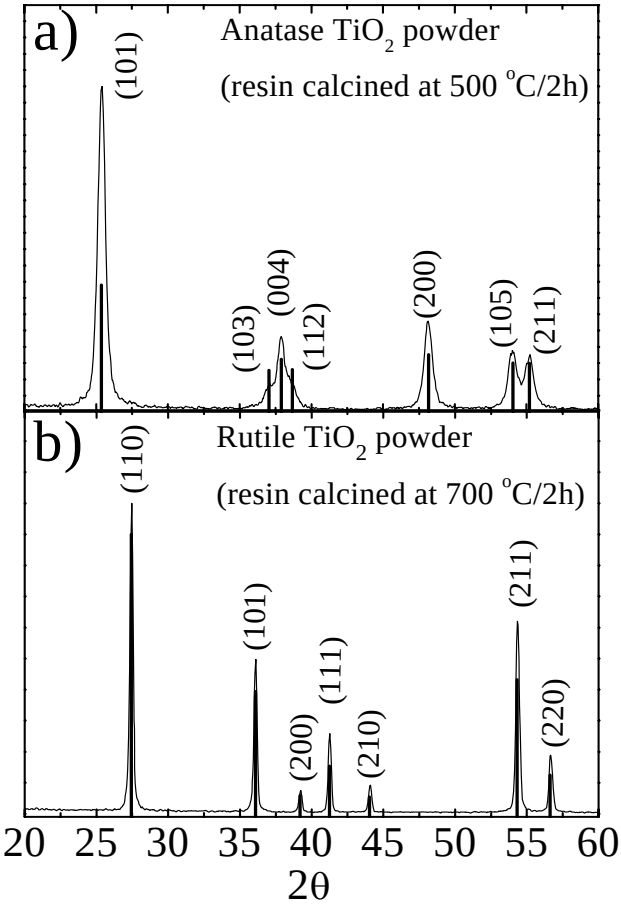

Figure 4 – XRD pattern of the TiO_2 powder obtained by Pechini's method. a) TiO_2 resin calcined at 500°C/2h resulting in anatase; and b) TiO_2 resin calcined at 700°C/2h, resulting in rutile. The vertical bars refer to the XRD pattern for anatase (JCPDS 78-2486) and rutile (JCPDS 77-0441) phases.

3.2 TiO_2 Films Characterization

The SEM-FEG micrograph presented in Figure 5 shows the 320 nm-thick film surface morphology. The film is free of cracks and has smooth surface morphology even for different regions analyzed. Both 320 nm-thick and 80 nm-thick films presented high optical quality. The 80-nm thick film is visually yellow coloured and the 320 nm-thick film is red coloured, being this difference due to the interference of light related to the film thickness.

The Figure 6 gives the transmittance spectra in the 300-1500 nm region for the films (subtracted the quartz substrate spectra). The 80 nm-thick film has transmittance of 91 % at 420 nm, 59 % at 750 nm, and 75 % at 1500 nm. The 320 nm-thick film has transmittance of 85 % at 420 nm, 88 % at 750 nm, and 95 % at 1500 nm. The interference pattern of the light can be observed in the form of oscillations that are present in both transmittance spectra, and are due to the interference between two interfaces; the air-film and film substrate.

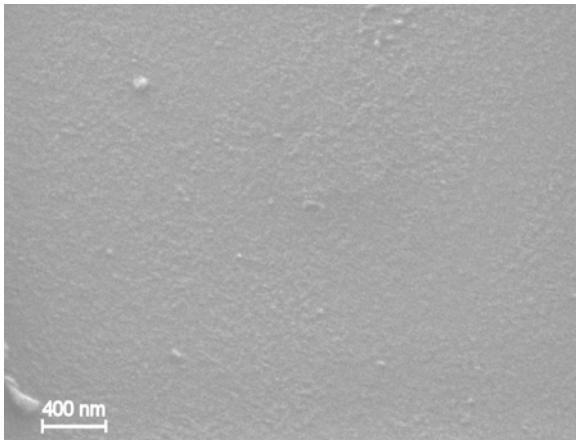

Figure 5 – SEM-FEG micrograph of the 320 nm-thick TiO_2 film deposited by EB-PVD of the powder obtained by pechini's method (25.000X magnification).

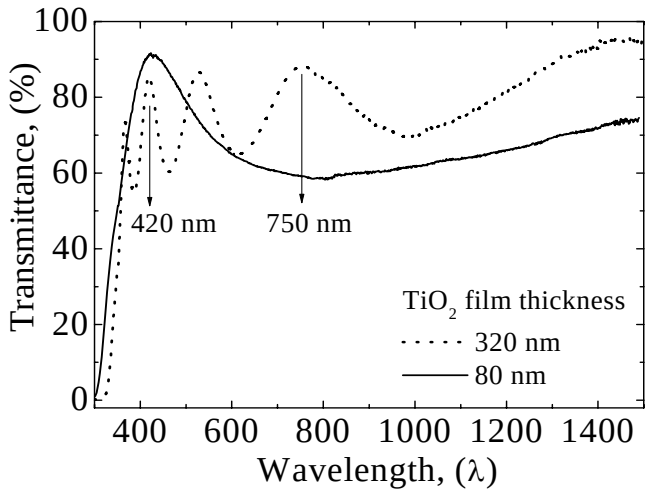

Figure 6 – Optical Transmittance spectra of 80 nm-thick (solid line) and 320 nm-thick (dotted line) TiO_2 films deposited by electron beam evaporation.

In Figure 7 is presented the Raman spectra of the TiO_2 powders and films obtained. The Raman peaks at 144.7, 196, 397, 515.7, and 637.2 cm^{-1} are characteristics of the anatase phase and the peaks at 238.5, 447.9, and 612.1 cm^{-1} correspond to the rutile phase. The Raman spectra of the thick and thin film (Fig 7-a and 7-b) presented the same peaks as observed for anatase powder (Fig 7-c).

The Figure 8 shows the XRD pattern of the TiO_2 films deposited by electron beam evaporation on quartz substrates submitted at 350 °C during the evaporation.

Using the quartz substrates submitted at 350 °C during the evaporation to favour adhesion and crystallization, the films presented only anatase phase, however in the 320 nm-thick film is possible to observe a preferential orientation in the (004) crystallographic direction. The 80 nm-thick and the 320 nm-thick films have average crystallite diameter of ~12 nm and ~19 nm, respectively, which

were estimated by the Scherrer's equation using the XRD from the Figure 8.

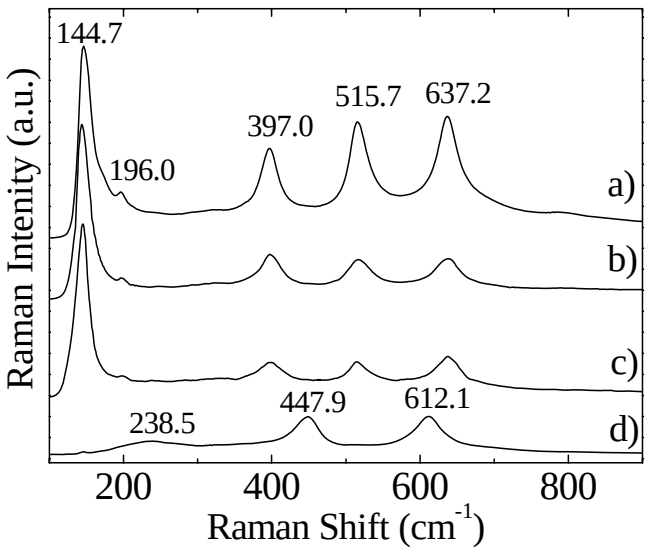

Figure 7 – Raman spectra of TiO_2 films and powders: a) 320 nm-thick, b) 80 nm-thick, c) Anatase powder, and d) Rutile powder.

The Figure 9 shows the AFM images obtained with scan of 5x5 μm of the TiO_2 films surface. Images obtained on different regions of the samples showed that the films exhibit a homogeneous globular structure. The entire film surface is formed by small grains of the deposited material. The average dimension of these particles was found to be 140 nm (from 80 nm to 200 nm) for the 80 nm-thick film (Fig. 9-a) and of 350 nm (from 250 nm to 450 nm) for the 320 nm-thick film (Fig. 9-b).

Also the TiO_2 films presented smooth surface morphology with average roughness (R_a) of 1.08 nm and 2.14 nm for the 80 nm-thick and the 320 nm-thick film, respectively. This significant increase in the average roughness can be attributed to the longer deposition time with substrate heated at 350 ^oC to produce the 320 nm-thick film (~ 60 min of deposition at 1.0 Å/s), compared to the 80 nm-thick film (~ 15 min of deposition at 1.0 Å/s), favouring the nucleation process and some kind of texturing of the grains on the thick film.

Moreover, these roughness values are smaller than those reported in the literature (~ 4 nm) for optically smooth TiO_2 films obtained by Sol-Gel [23,24], Metal Plasma Immersion [25], and Sputtering technique [26]. Complementarily, to the observed increase in the roughness, a grain orientation perpendicular to the substrate plane was observed for the 320 nm-thick film as shown in the Figure 9-d. This result is in agreement with the increase in the (004) orientation also observed in the XRD pattern (Fig 8-b) due to the increase in the intensity of the peak at 37.9, as earlier mentioned.

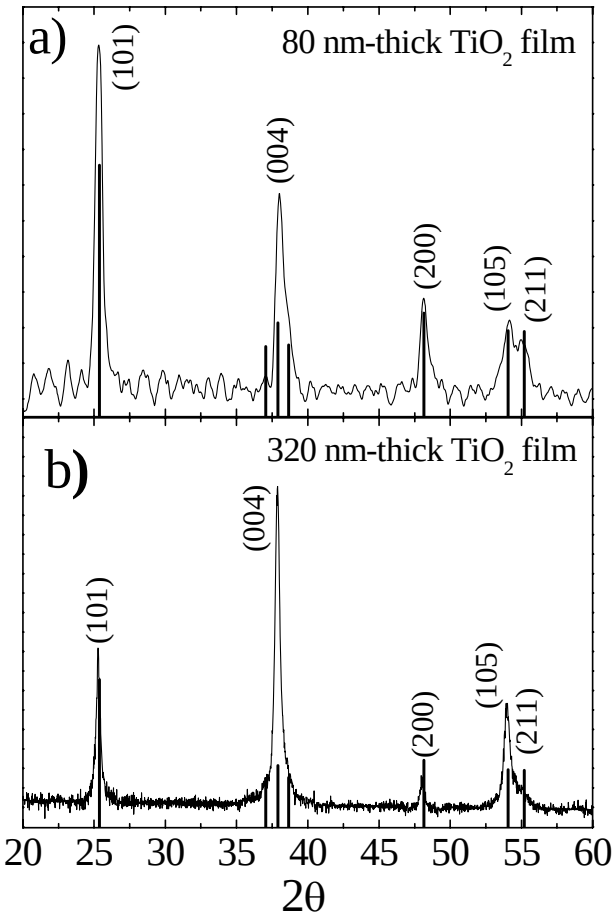

Figure 8 – X-ray diffraction pattern of TiO_2 films deposited by electron beam evaporation a) 80 nm-thick, and b) 320 nm-thick. The vertical bars refer to the XRD pattern for anatase (JCPDS 78-2486) phase.

4. CONCLUSION

In this work we presented the synthesis of nanometric anatase and rutile TiO_2 phases obtained with low temperature calcinations of a TiO_2 resin prepared using the Pechini's method. Anatase phase with average particle size of 60 nm and average crystallite size of 13 nm was obtained firing the TiO_2 resin at 500 ^oC/2h, and rutile phase with average crystallite size of 34 nm was achieved firing the TiO_2 resin at 700 ^oC/2h, as measured by XRD.

Transparent, optically smooth and homogeneous TiO_2 films with thickness of 80 nm and 320 nm were produced by electron beam vacuum deposition, starting from nanometric TiO_2 powder obtained by Pechini's method. The films were deposited on amorphous quartz substrates heated at 350 ^oC during the evaporation, and presented anatase phase. Roughness value of 1.08 nm and 2.14 nm was obtained, for the 80 nm-thick and 320 nm-thick film, respectively. The films roughness value (R_a) obtained is low compared with values (~ 4 nm) presented in the literature [23-26] for TiO_2 films produced by other deposition techniques.

The 320 nm-thick film presented increased grain size and large roughness attributed to the longer time of

deposition with substrate heated at 350 °C, causing nucleation and texturing of the grains, observed by XRD and AFM. The films presented only anatase phase investigated by XRD and MicroRaman spectroscopy.

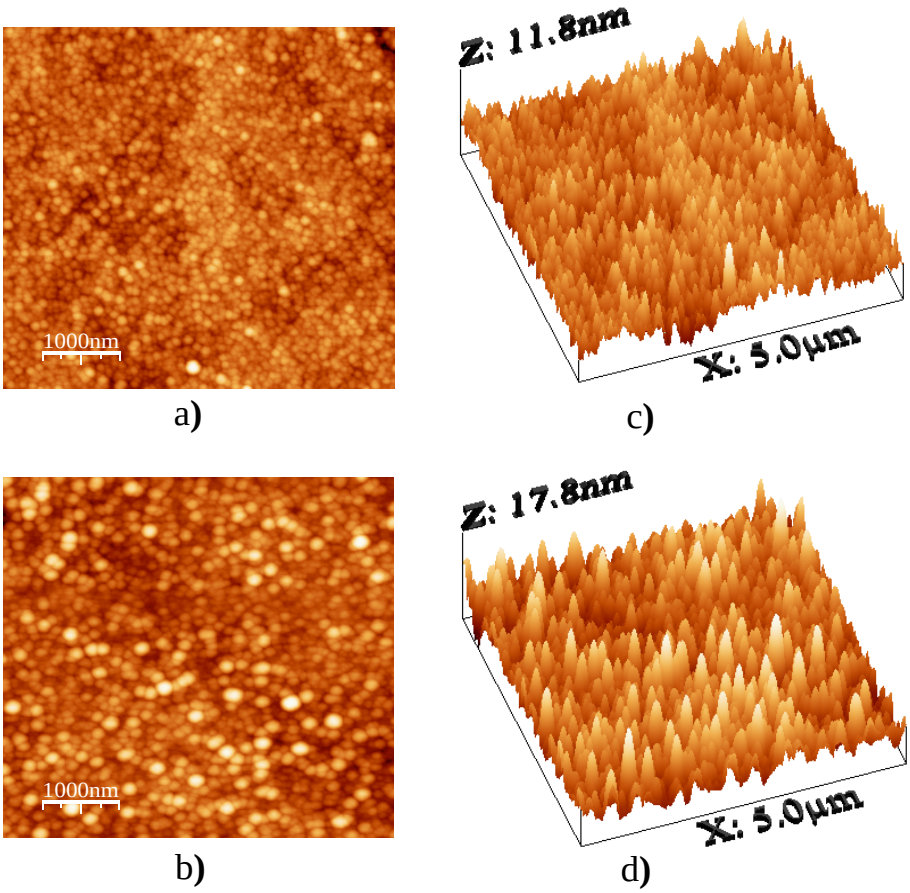

Figure 9 – AFM images of the surface morphology of the TiO_2 films produced by electron beam evaporation on amorphous quartz substrates submitted at 350 °C during the deposition. a) 80 nm-thick film 2D image, b) 320 nm-thick film 2D image, c) 80 nm-thick film 3D image (R_a=1.08 nm), and d) 320 nm-thick film 3D image (R_a=2.14 nm). The 3D images show the grain orientation details on the film surface.

ACKNOWLEDGEMENTS

The authors acknowledge the financial support received from the Brazilian Agencies, FAPESP (04/11905-5), CAPES, and CNPq. We also thanks to Prof. Dr. Máximo Siu Li for availability of the EB-evaporation system, and Dr. Carlos A. Baldan from Faculdade de Engenharia Química de Lorena, for providing the Tantalum crucibles used for electron beam evaporation. Also to Prof. Dr. Antonio Ricardo Zanatta for the MicroRaman measurements.

REFERENCES

1. WANG, R.; SAKAI, R.; FUZISHIMA, A.; WATANABE, T.; HASHIMOTO, K., *J. Phys. Chem*. B 103 (1999) 2188.
2. HAO, Y.; YANG, M.; YU, C.; CAI, S.; LIU, M.; FAN, L.; LI, Y., *Solar Energy Mater. Solar Cells* 56 (1998) 75.
3. MURAKOSHI, K.; KOGURE, R.; WADA, Y.; YANAGIDA, S., *Chem. Lett*. (5) (1997) 471.
4. WANG, G.; CHEN, H.; ZHANG, H.; YUAN, C.; LU, Z.; YANG, W., *Appl. Surf. Sci*. 135 (1998) 97.
5. KOBAYASHI, N.; TESHIMA, K.; HIROHASHI, R., *J. Mater. Chem*. 8 (1998) 497.
6. HUANG, N.; CHEN, Y.; LUO, J.; YI, J.; LU, R.; XIAO, J.; XUE, Z.; LIU, X., *J. Biomater. Appl*. 8 (1994) 404.
7. LARSSON, C.; THOMSEN, P.; LAUSMAA, J.; RODAHL, M.; KASEMO, B.; ERICSSON, L.E., *Biomaterials* 15 (1994) 1062.
8. HENGLEIN, A., *Chem. Rev*. 89 (1989) 1861.
9. WELLER, H., *Angew. Chem. Int. Ed. Engl*. 32 (1993) 41.
10. CHEN, C.C.; HERHOLD, A.B.; JOHNSON, C.S.; ALIVISATOS, A.P., *Science* 276 (1997) 398.
11. SINHA, S.K., *Appl. Surf. Sci*. 182 (2001) 176.
12. LI, W.; SHAH, S.I.; SUNG, M.; HUANG, C.P.; *J. Vac. Sci. Technol. B* 20 (2002) 2303.

13. ILISZ, I.; DOMBI, A.; MOGYOROSI, K.; DEKANY, I.; *Colloids and Surfaces A: Physicochem. Eng. Aspects* 230 (2003) 89.
14. NIEDERBERGER, M.; GARNWEITNER, G.; KRUMEICH, F.; NESPER, R.; COLFEN, H.; ANTONIETTI, M., *Chem. Mater.* 16 (2004) 1202.
15. CARP, O.; HUISMAN, C.L.; RELLER, A., *Prog. in Sol. Sta. Chem.* 32 (2004) 33–177.
16. LIN, Y.H.; ZHANG, Z.T.; HUANG, S.L.; LI, J.L., *J. of Inorg. Mat.* 14 (6) (1999) 853.
17. LI, B.R.; WANG, X.H.; YAN, M.Y.; LI, L.T., *Mat. Chem. and Phys.* 78 (1) (2003) 184
18. LEE, Y.C.; JUNG, Y.J.; PARK, P.Y.; KO, K.H., *J. of Sol-Gel Sci. and Technol.* 30 (1) (2004) 21.
19. OHRING, M., *Materials Science of Thin Film - Deposition and Structure*, Academic Press, 1992 , (see pp.63-65).
20. DE VICENTE, F.S.; RUBO, E.A.A.; SIU LI, M., *Revista Brasileira de Aplicações de Vácuo*, 23 (2004) 11.
21. OLIVEIRA, M.M.; SCHNITZLER, D.C.; ZARBIN, A.J.G., *Chem. Mater.* 15 (2003) 1903.
22. GROSA, J.R., *NanoStructured Materials*, 12, (1999) 987.
23. CHRYSICOPOULOU, P.; DAVAZOGLOU, D.; TRAPALIS, C.H.R.; KORDAS, G., *Thin Solid Films*, 323 (1998) 188.
24. ZAHARESCU, M.; CRISAN, M., *J. of Sol-Gel Sci. and Technol.*, 13 (1998) 769.
25. TSYGANOV, I.; MAITZ, M.F.; WIESER, E.; PROKERT, F.; RICHTER, E.; ROGOZIN, A., *Surf. Coat. Technol.* 174-175C (2003) 591.
26. KARUNAGARAN, B.; MANGALARAJ, D.; KIM, K.; HONG, B.; ROH, Y.; SEOK, P.C.; YI, J., *Cryst. Res. Technol.* 40 (3) (2005) 222.